The Relationship among Complex Fractionated Electrograms, Wavebreak, Phase Singularity, and Local Dominant Frequency in Fibrillation Wave-Dynamics: a Modeling Comparison Study

Yonghyeon Yun,[1]* Minki Hwang,[2]*
Jae Hyung Park,[2] Hangsik Shin,[3]
Eun Bo Shim,[4] and Hui–Nam Pak[2]

[1]Department of Convergence Biomedical Engineering, Daelim University College, Anyang; [2]Division of Cardiology, Yonsei University Health System, Seoul; [3]Department of Biomedical Engineering, Chonnam National University, Yeosu; [4]Department of Mechanical and Biomedical Engineering, Kangwon National University, Chuncheon, Korea

*Yonghyeon Yun and Minki Hwang contributed equally to this work.

Although complex fractionated electrogram (CFE) is known to be a target for catheter ablation of fibrillation, its physiological meaning in fibrillation wave-dynamics remains to be clarified. We evaluated the spatiotemporal relationships among the parameters of fibrillation wave-dynamics by simulation modeling. We generated maps of CFE-cycle length (CFE-CL), local dominant frequency (LDF), wave break (WB), and phase singularity (PS) of fibrillation in 2-dimensional homogeneous bidomain cardiac modeling (1,000 × 1,000 cells ten Tusscher model). We compared spatiotemporal correlations by dichotomizing each maps into 10 × 10 lattice zones. In spatial distribution, WB and PS showed excellent correlation (R = 0.963, P < 0.001). CFE-CL had weak correlations with WB (R = 0.288, P < 0.001), PS (R = 0.313, P < 0.001), and LDF (R = -0.411, P < 0.001). However, LDF did not show correlation with PS or WB. PSs were mostly distributed at the periphery of low CFE-CL area. Virtual ablation (5% of critical mass) of CFE-CL < 100 ms terminated fibrillation at 14.3 sec, and high LDF ablation (5% of critical mass) changed fibrillation to organized tachycardia, respectively. In homogeneous 2D fibrillation modeling, CFE-CL was weakly correlated with WB, PS, and LDF, spatiotemporally. PSs are mostly positioned at the periphery of low CFE-CL areas, and virtual ablation targeting low CFE-CL regions terminated fibrillation successfully.

Keywords: Fibrillation; Complex Fractionated Electrogram; Simulation Modeling

INTRODUCTION

In 2004, Nademanee et al. reported that catheter ablation of atrial fibrillation (AF) targeting complex fractionated atrial electrograms (CFAE) was effective in terminating and preventing AF (1). He also declared that epicardial catheter ablation targeting complex fractionated electrogram (CFE) reduces ventricular fibrillation (VF) or sudden cardiac death in Brugada syndrome (2). Sophisticated mapping and ablation of CFAE based on CFE-cycle length (CL) or rotor is known to improve the clinical outcomes of AF catheter ablation (3), and the 2012 HRS/ERHA/ECAS Expert Consensus Statement (4) recommended performing CFAE guided ablation in addition to conventional circumferential pulmonary vein isolation in patients with long-standing persistent AF.

Previously, we also reported that the area of CFE is associated with low voltage areas, as well as slow conduction velocity, in humans (5). However, the physiological meaning of CFE and why CFE guided ablation is effective have not yet been elucidated. The main difficulties encountered in physiologic studies of CFE are as follows: 1) CFE is acquired from local bipolar electrograms, and simultaneous acquisition from multiple mapping points is not clinically available. 2) With limited resolution in clinical electroanatomical mapping techniques, it is difficult to realize parameters for quantifying fibrillation wave dynamics, such as wave-break point (WB) or phase singularity point (PS) without surgical high density mapping. Therefore, in this study, we attempted to study CFE electrograms generated by virtual bipolar electrogram via in silico simulation modeling, comparing spatiotemporal distributions of WB, PS, and local dominant frequency (LDF).

The purpose of this study was to evaluate the meaning of CFE-CL in fibrillation wave-dynamics, comparing WB, PS, and LDF spatiotemporally. We also investigated the effect of virtual

ablation targeting CFE and LDF.

MATERIALS AND METHODS

2D bidomain fibrillation modeling

A 2D bidomain fibrillation model for computer simulation were implemented using Microsoft visual C++ version 10.0 (Microsoft Co., Redmond, WA, USA) and MATLAB ver. 7.13 (MathWorks Co., Natick, MA, USA). The source code of the cell model was from the CellML version and already implemented in our previous computational studies (6-8). The solution algorithm for the bidomain method was from Ashihara et al. (9). A 1,000 × 1,000 element cell array was used to simulate fibrillation waves based on a ten Tusscher-Panfilov model (10) which describes the intracellular ion dynamics in more detail than Priebe-Beuckelmann (11) type model, and computationally more efficient than Iyer-Mazhari-Winslow (12) model (13). A spatial discretization of 0.25 mm and a temporal discretization of 0.05 ms were used for all simulations, and data were sampled every 1 ms. A finite element formulation using the Galerkin method (14) was used for the discretization of the bidomain equations for electric wave propagation in tissue. We chose diffusion coefficients of 0.00462 cm^2/s for intracellular cellular portions and 0.00154 cm^2/s for extracellular portions. No electric flux condition was

applied for all the boundaries of intra- and extracellular domains. For the re-entry initiation, we used the protocol of Clayton and Holden (15) which we validated previously (8). In our 2D bidomain modeling, action potential duration at 90% repolarization (APD90) was 304 ms and conduction velocity was 0.58 m/s at 600 ms pacing cycle length (CL; Fig. 1A and C).

Generation of virtual bipolar electrogram and CFE

As a bipolar electrogram is needed to generate CFE, we designed virtual bipolar catheter simulating currently utilized clinical one (Celsius, model DI7TCBLRT, Johnson and Johnson Inc. Diamond Bar, CA, USA, Fig. 1B). The sizes of the distal electrode and proximal electrode were 3.5 mm × 2.0 mm and 1.5 mm × 2.0 mm, respectively. The inter-electrode distance was 1.0 mm, and we oriented the distal and proximal electrodes with consistent vertical directivity (top to bottom). We averaged the whole action potentials recorded within each virtual electrode areas, and generated virtual bipolar electrograms by subtracting the amplitudes of averaged potentials from each electrode and filtering with a band-pass of 30-200 Hz (Fig. 1D). The virtual catheter device sweeps every mesh point to compute point-by-point electrogram. CFE-CL was calculated from electrogram data collected for 6 sec by measuring the time intervals between multiple and discrete deflections at the maximum negative dV/dt
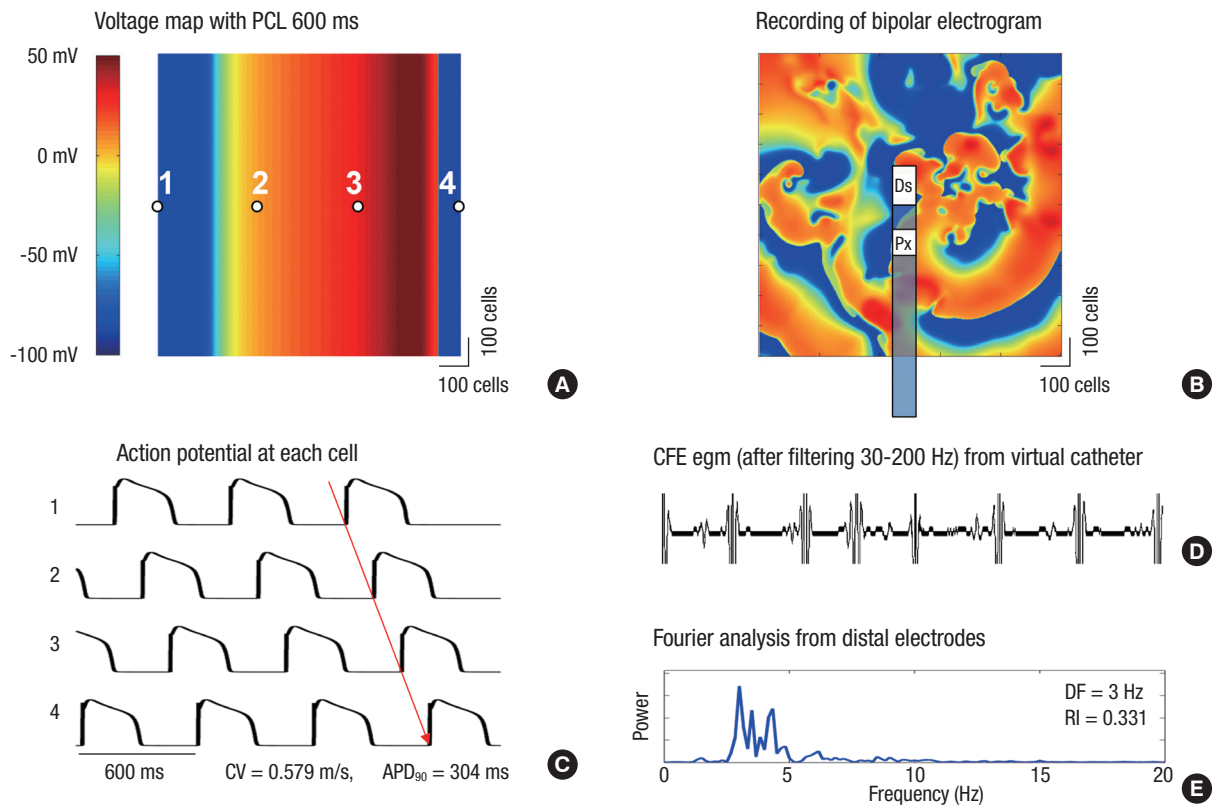

Fig. 1. Voltage map and complex fractionated electrogram (CFE) acquisition using virtual bipolar electrodes. (A) Voltage map with pacing cycle length (PCL) 600 ms and its action potential. (B) Recording of bipolar electrogram and CFE from virtual catheter. (C) Recording of action potential at each cell and activation pattern. (D) Virtual bipolar egm showing CFEs. (E) Local dominant frequencies generated from the locations of distal and proximal electrodes by Fourier analyses. Ds, Distal electrode; Px, Proximal electrode.

and averaging inter-deflection time intervals. An adaptive peak-to-peak sensitivity threshold was not considered, because the data comprised simulation data without noise. The refractory period was set to 40 ms and the duration for preventing far-field events was set at 15 ms (16).

Determination of WB, PS, and LDF

WB was defined as a point where the wave-front and wave-tail met (17) on the pseudo action potential map. Wave-fronts were detected by the maximum dV/dt in phase 0 of an action potential curve, and wave-tails were defined as points of 50% repolarization. Wave-fronts are tracked, and when the wave-front meets a wave-tail, the point is determined to be WB. Phase of action potential, θ(t), was calculated as the arctangent of V_m (t)-V_{m_MEAN} over V_m (t+τ)-V_{m_MEAN}, where V_m (t) is the voltage of cardiac action potential at t seconds and τ is the embedding delay (30 ms). PS was defined as the point where the phase was undetermined or ambiguous, and was detected by Iyer-Gray's algorithm (18). PS also includes the points where the phase is undetermined.

LDF was analyzed by the power spectra density function using a Hanning window (19) and discrete Fourier transform over a 6 sec duration of virtual action potential recording for each cell, and defined as the frequency of the maximum peak power within 1-20 Hz.

Spatiotemporal correlation methods for CFE, WB, PS, and LDF

Based on the above algorithm, we generated color-coded WB, PS, LDF and CFE-CL maps using data collected during 8-14 sec, 14-20 sec, 20-26 sec, and overall 8-26 sec data of fibrillation (Fig. 2). Data collected during the first 0-8 sec were excluded due to the potential instability of wave-dynamics immediately after induction of fibrillation. For the spatial comparisons of each parameter (WB, PS, LDF, and CFE-CL), we divided each color map into 10 × 10 lattice zones (100 × 100 cells in each zone) for the same time period, and the mean values of each parameter in each lattice zone were calculated and analyzed spatially.
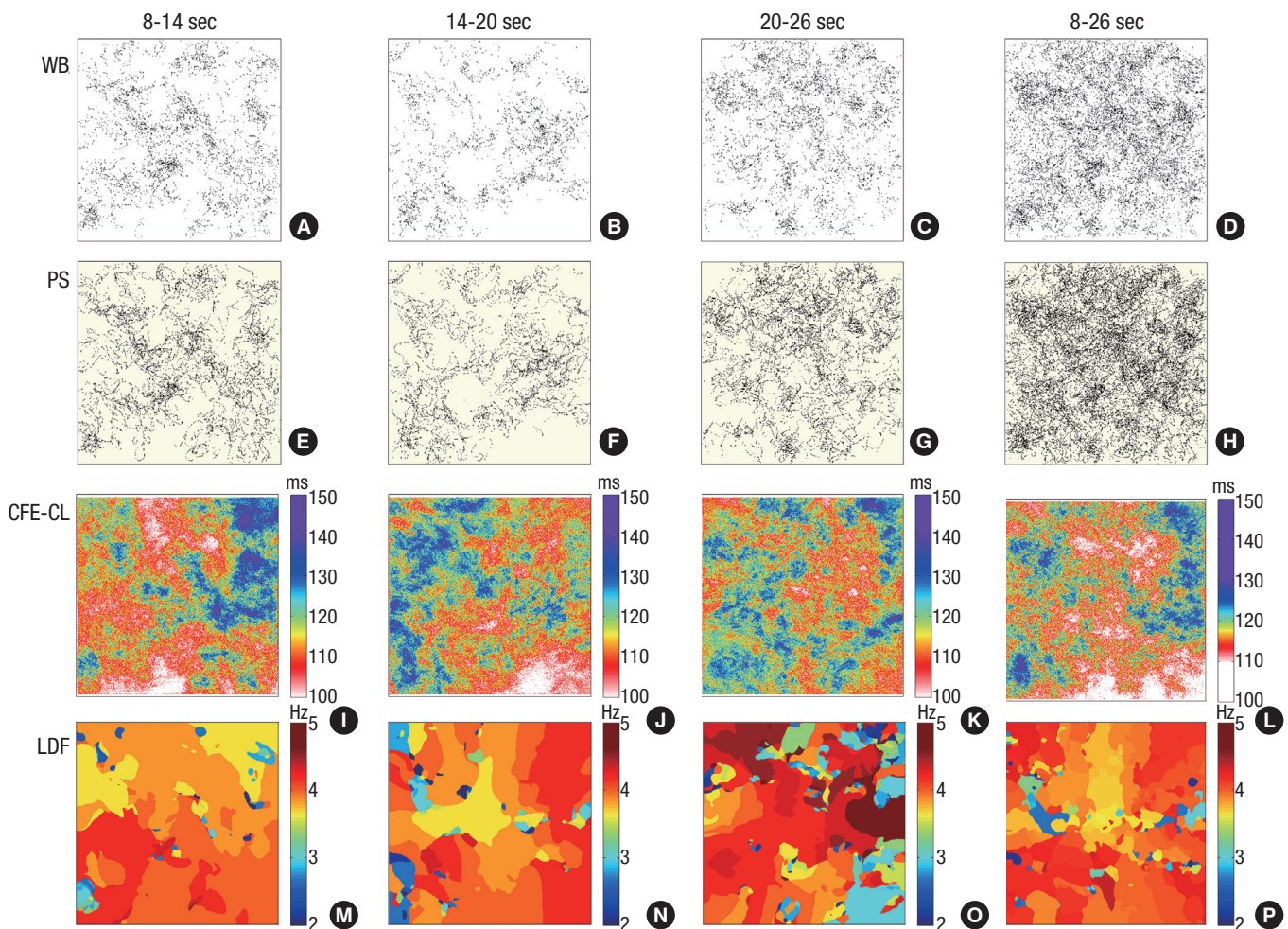

Fig. 2. Spatiotemporal distributions of wavebreak (WB), phase singularity (PS), local dominant frequency (LDF), and complex fractionated electrogram-cycle length (CFE-CL) in multiple time intervals. WB and PS maps display cumulative points during the corresponding periods of fibrillation. Maps of CFE-CL and LDF are color-coded according to the color scale bars.
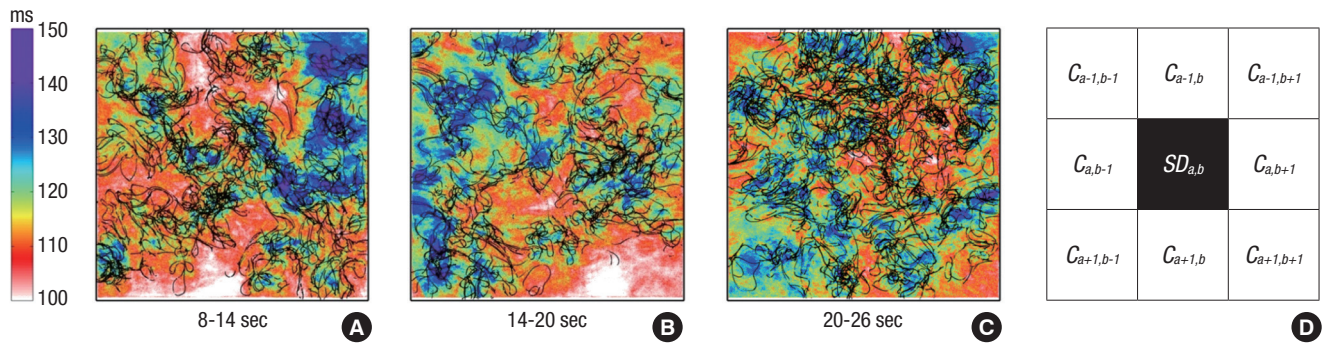
Fig. 3. Overlap of complex fractionated electrogram-cycle length (CFE-CL) and phase singularity (PS). (**A**-**C**) Overlaying of CFE-CL maps and cumulative PS maps of 6 sec durations of fibrillation. PS are mostly positioned at the periphery of areas with short CFE-CL. (**D**) Calculating methods for standard deviation of CFE-CL around the cell of interest. Standard deviation of CFE-CL at the cells around PS were compared with that around non-PS. "a-1, b-1, a+1, and b+1" indicate coordinates of cells.

Overlaying PS on CFE-CL maps and virtual CFE and LDF ablations

To investigate the relationship of spatial distribution between PS and CFE, we projected PS on CFE maps (Fig. 3), and compared CFE-CL distribution at the periphery of PS sites vs non-PS sites. In consideration of a size mismatch between virtual electrodes and cells, CFE-CL at the central cell of virtual catheter was used as a representative value, and we compared standard deviations of CFE-CL from 8 cells around the cell of interest (Fig. 3D). To conduct virtual CFE and LDF ablation, both CFE-CL and LDF values at each site were sorted in ascending order, and the cells of the upper 5% of short CFE-CL and high LDF were ablated respectively, to minimize the effect of critical mass reduction. Ablation was done by setting the ionic current conductance to zero and membrane potential to the baseline (-86.2 mV).

Statistical analyses

Data are expressed as mean ± standard deviation. Linear correlation was evaluated to prove the relationship among WB PS, LDF, and CFE, both spatially and temporally. The standard deviation of CFE-CL at PS sites and non-PS sites were compared quantitatively by Student's t-test. A *P* value of < 0.05 was considered statistically significant.

RESULTS

Spatial correlation of CFE vs WB, PS, and LDF

In this study, we were able to generate virtual bipolar electrograms with the algorithm described above and demonstrated CFE during fibrillation (Fig. 1D). Fig. 2 compares the spatial distributions of WB, PS, CFE-CL, and LDF, depending on the recording timing during fibrillation. For the 6 sec cumulative maps of WB and PS, their spatial distributes were very similar, but seemed to spare the area with short CFE-CL (Fig. 2I and J). At 20-26 sec, WB and PS distribution spread over the mapped area (Fig. 2C and G), and there was no significantly localized short CFE-CL area (Fig. 2K). However, a prominent high LDF area was

observed, as shown in Fig. 2O. For 8-26 sec fibrillation data, areas of WB and PS were not localized, and neither were localized on the area of LDF. Although we observed sustained rotors in activation map from time to time, there was no stationary PS or WB sustaining longer than 6 sec. For statistical analyses, mean values of each parameter at 100 evenly divided lattice zones in three different serial time durations were compared and correlated. Accordingly, WB and PS exhibited very nice correlation to each other (Fig. 4A), and CFE-CL showed weak correlations with LDF, PS, and WB, respectively (Fig. 4D to F). However, LDF did not show any correlation with PS or WB (Fig. 4B and C).

PS positioned at the periphery of short CFE-CL Areas

As shown in Fig. 3, PS are positioned at the boundary of short CFE-CL areas, sparing the shortest CFE-CL area. We evaluated CFE-CLs around the cells with PS (PS area) and those without PS (non-PS area) to prove spatial relationships between CFE and PS. In statistical analysis, the standard deviation value of CFE-CL was significantly higher at cells with PS than at cells without PS, suggesting PS is more likely to be localized at areas of CFE-CL change than non-PS cells (*P* < 0.001, Table 1). This finding was consistent temporarily (Fig. 3A to C), and PS tracked the boundary of the shortest CFE-CL area.

CFE Ablation terminated fibrillation, but LDF ablation organized fibrillation

In CFE-CL maps generated using 8-14 sec data, we plotted the upper 5% of the shortest CFE-CL cells and 5% critical mass of the highest DF area (Fig. 5). After plotting the mask area, we ablated the area of high DF (Fig. 5C) and short CFE-CL (Fig. 5D). In contrast the virtual DF ablation changed fibrillation to organized tachycardia, CFE ablation organized and finally terminated fibrillation in 14.3 sec.

DISCUSSION

In this study, we were able to realize virtual CFE and evaluate its meaning in fibrillation wave-dynamics by 2D bidomain ho-
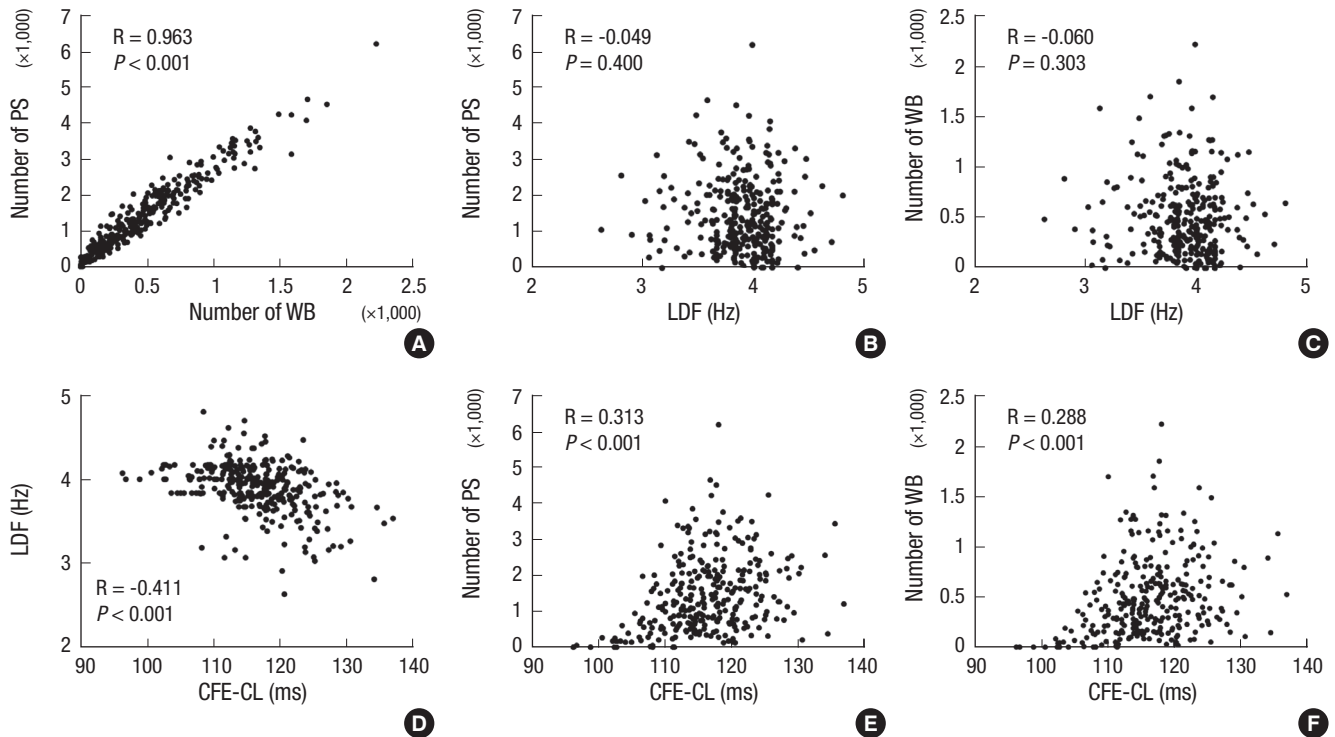
Fig. 4. Spatiotemporal correlations among wavebreak (WB), phase singularity (PS), local dominant frequency (LDF) and complex fractionated electrogram-cycle length (CFE-CL) (n=300).

Table 1. Differences in spatial standard deviation of CFE-CL at neighboring PS and non-PS sites

Time (sec)	Parameter	PS	NPS	P value
8-14	Number of cells	70,872	895,353	< 0.001
	SD of CFE-CL (ms)	4.320 ± 1.415	4.082 ± 1.348	
14-20	Number of cells	51,974	914,251	< 0.001
	SD of CFE-CL (ms)	4.375 ± 1.372	4.109 ± 1.326	
20-26	Number of cells	86,875	879,350	< 0.001
	SD of CFE-CL (ms)	4.337 ± 1.350	4.188 ± 1.305	

PS, phase singularity point area; NPS, non-phase singularity area; SD, standard deviation; CFE-CL, cycle length of complex fractionated electrogram.

mogeneous cardiac simulation modeling. Briefly, we observed high spatial correlation between WB and PS, and weak correlations between CFE-CL and WB, PS, or LDF. However, LDF was not shown to be correlated with WB or PS. Additionally, PS was shown to be positioned mostly at the periphery of areas with the shortest CFE-CL or CFE-CL change. Lastly, virtual ablation targeting CFE terminated fibrillation successfully.

Konings et al. (20) reported that CFAE areas were mostly observed at areas of slow wave conduction and/or at pivot points of wavelet turn-around. Afterwards, Nademanee et al. (1) suggested a clear definition of CFAE as 1) fractionated electrograms composed of two or more deflections and/ or a perturbation of the baseline with continuous deflection of prolonged activation complex, and 2) atrial electrograms with a very short CL ($\leq$ 120 ms). In patients with ischemic cardiomyopathy, CFEs were fre-

quently recorded at the infarct border zone inside or outside of the ventricular tachycardia foci (21). However, it is more commonly found in patients with ischemic ventricular tachycardia than those without (22). Nademanee et al. (2) also reported that normalization of a Brugada pattern ECG in 89% after CFE-guide ablation in ventricular tachycardia/ventricular fibrillation (VT/VF) in patients with Brugada syndrome and 78% long-term suppression of ventricular tachyarrhythmias.

There are two major theories that explain the maintenance mechanism of fibrillation, the multiple wavelet hypothesis (17) and focal source hypothesis (23). The multiple wavelet theory suggests that continuous break-up of wavelets and co-existing 4-6 spiral wave cores maintain fibrillation, generating WB or PS. In contrast, the focal source hypothesis advocates that a high-frequency mother rotor generates fibrillatory conduction. Wu et al. (24) proved that both multiple wavelets and a mother rotor can exist in the same heart depending on conduction pattern, and Pak et al. (25) further emphasized the importance of the anatomical structure of this wave-dynamics pattern. In clinical practice, CFE targeted ablation exerts antiarrhythmic effects, but its meaning in fibrillation wave-dynamics has not yet been evaluated. Studies regarding CFE and wave-dynamics are limited to conduct, because of the low spatio-temporal resolution of bipolar electrograms and difficulty in excluding the effects of anatomical characteristics or anisotropy. In this study, we demonstrated a relatively weak spatial correlation between
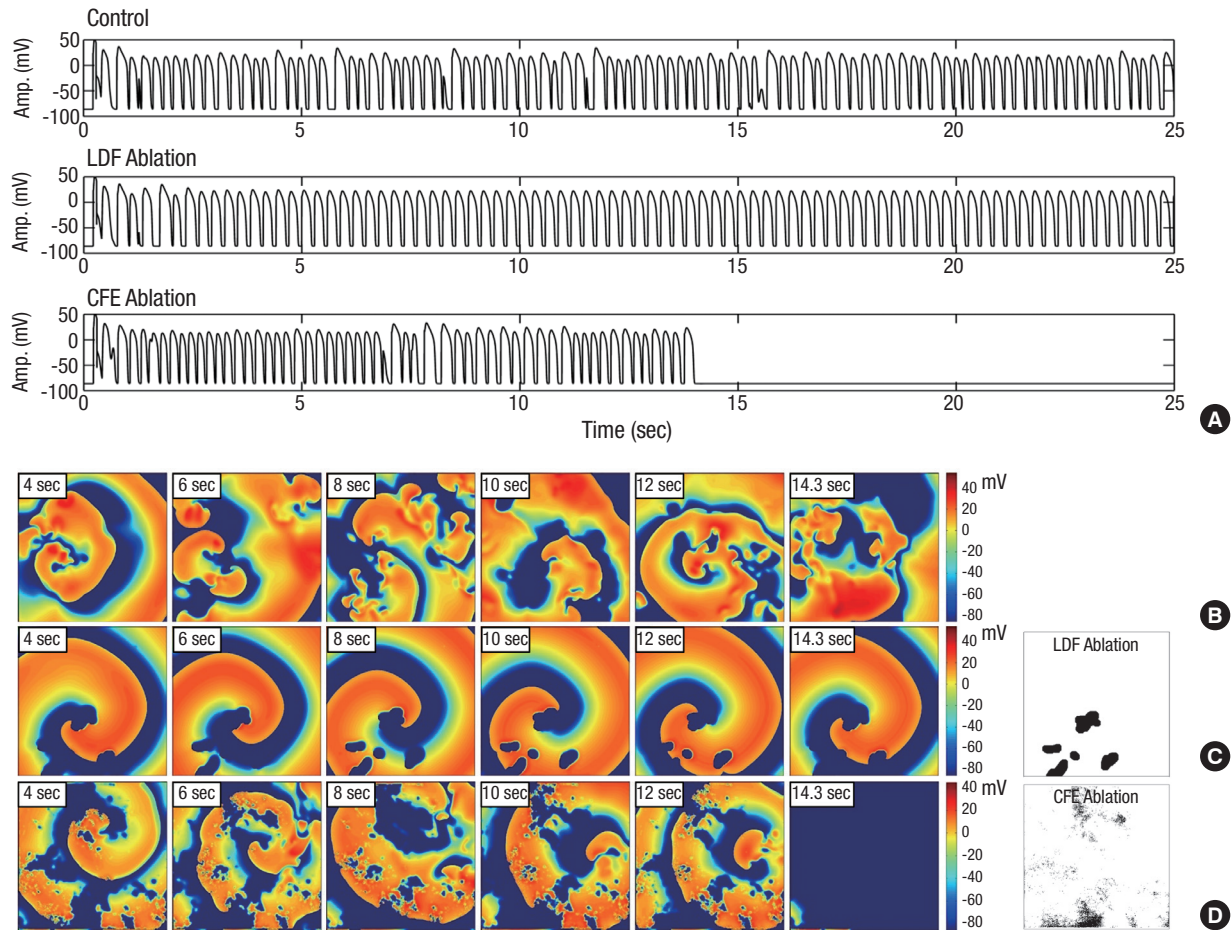
Fig. 5. Complex fractionated electrogram (CFE)-guided ablation. (A) virtual action potential curves during fibrillation/tachycardia in control, after local dominant frequency (LDF) ablation, and after CFE ablation, respectively. (B) Spatiotemporal changes of voltage maps of control fibrillation. Time duration after induction is marked on left upper part of each voltage map. (C) After virtual ablation of LDF (5% of critical mass; far right panel), fibrillation changed to sustaining organized tachycardia. (D) After virtual CFE ablation (5% of critical mass; far right panel), fibrillation terminated spontaneously in 14.3 sec.

CFE and WB, PS, or LDF via a 2D homogeneous monolayer cardiac simulation model, excluding other confounding effects. Although there has been report the multicomponent continuous electrogram surrounds high DF area in human atrium (26), PS was not associated with high LDF area. Therefore, CFE might be associated with both active driver, such as mother rotor, and passive wavebreaker, such as collision of multiple wavelets, at the virtual condition excluding anatomical or histological characteristics. In contrast the virtual DF ablation changed fibrillation to organized tachycardia, CFE ablation gradually organized fibrillation and finally terminated it in our model. Both types of ablation had anti-arrhythmic effects with different mechanisms. We speculate that LDF ablation eliminated passive wave-breakers, but CFE ablation might target core of the fibrillation. Further study is warranted for the mechanism of virtual ablation and whether CFE ablation eliminated rotor or mother focus.

After Hodgkin and Huxley described action potential with a mathematical model (27), much research has been put into a model of human cardiac cells; moreover, computer models of cardiac electrophysiology have been developed to organ scales with parallel computing technology. Computer simulation modeling will fill the gap between clinical electrophysiology and sophisticated basic arrhythmia research. Furthermore, in silico models may be applicable to practical purposes, such as appropriate targeting of virtual ablation, estimation of cardiac resynchronization effects, or development of parameters to predict arrhythmia risk. It may also be able to provide clues in evaluating calcium associated wave-dynamics or mechano-electrical feedback. To achieve such goals, the development of physiologic and highly efficient modeling, integration of patient specific electroanatomical information, and creation of sophisticated analytic software are warranted.

Although CFE guided ablation has been mostly applied in atrial fibrillation, we used ten Tusscher-Panfilov model (10) which is a ventricular modeling. Though our previous studies suggest that fractionated electrogram guided ablation may terminate or reduce inducibility of ventricular fibrillation (28), the present study results may not be applicable to atrial wave dy-

namics. We are currently conducting a separate study using a human atrial cell model.

This study aims to apply clinical CFE ablation to a simulation model and to propose a new methodology to build a bridge between clinical approach and basic science of computer simulation. This study was conducted via 2D in silico modeling comprising a single cell layer. However, atrial tissue is thinner than ventricular tissue, and the role of transmural reentry is not as great as in ventricular models. Furthermore, our simulation modeling did not reflect anatomical characteristics, tissue heterogeneity with 3D anisotropic structure or realistic fiber orientations. Our model was more likely to realize the multiple wavelet type of fibrillation than mother rotor dependent fibrillation. We consistently placed the virtual bipolar catheter on a vertical position in the mapped area; therefore, the distribution of CFE may vary for different catheter directions or inter-electrode intervals.

We successfully realized virtual CFE and virtual CFE targeted ablation during fibrillation. CFE-CL was spatially correlated with WB, PS, or LDF, respectively, and PS are mostly positioned at the periphery of short CFE-CL areas with CFE-CL change. Virtual ablation targeting short CFE-CL area did terminate fibrillation and high LDF ablation changed fibrillation to organized tachycardia in this in silico human cardiomyocyte model. Current clinical CFE ablation has electrophysiologically valid background, not a barely experience based destructive surgery.

DISCLOSURE

The authors do not declare any conflict of interest.

ORCID

Yonghyeon Yun http://orcid.org/0000-0001-5497-452X
Minki Hwang http://orcid.org/0000-0001-7404-3052
Jae Hyung Park http://orcid.org/0000-0002-3198-1134
Hangsik Shin http://orcid.org/0000-0002-3353-0310
Eun Bo Shim http://orcid.org/0000-0003-2657-0389
Hui-Nam Pak http://orcid.org/0000-0002-3256-3620

REFERENCES

1. Nademanee K, McKenzie J, Kosar E, Schwab M, Sunsaneewitayakul B, Vasavakul T, Khunnawat C, Ngarmukos T. *A new approach for catheter ablation of atrial fibrillation: mapping of the electrophysiologic substrate. J Am Coll Cardiol 2004; 43: 2044-53.*
2. Nademanee K, Veerakul G, Chandanamattha P, Chaothawee L, Ariyachaipanich A, Jirasirirojanakorn K, Likittanasombat K, Bhuripanyo K, Ngarmukos T. *Prevention of ventricular fibrillation episodes in Brugada syndrome by catheter ablation over the anterior right ventricular outflow tract epicardium. Circulation 2011; 123: 1270-9.*
3. Verma A, Sanders P, Macle L, Deisenhofer I, Morillo CA, Chen J, Jiang CY, Ernst S, Mantovan R. *Substrate and trigger ablation for reduction of atrial fibrillation trial-part II (STAR AF II): design and rationale. Am Heart J 2012; 164: 1-6.e6.*
4. Calkins H, Kuck KH, Cappato R, Brugada J, Camm AJ, Chen SA, Crijns HJ, Damiano RJ Jr, Davies DW, DiMarco J, et al. *2012 HRS/EHRA/ECAS expert consensus statement on catheter and surgical ablation of atrial fibrillation: recommendations for patient selection, procedural techniques, patient management and follow-up, definitions, endpoints, and research trial design: a report of the Heart Rhythm Society (HRS) Task Force on Catheter and Surgical Ablation of Atrial Fibrillation: developed in partnership with the European Heart Rhythm Association (EHRA), a registered branch of the European Society of Cardiology (ESC) and the European Cardiac Arrhythmia Society (ECAS); and in collaboration with the American College of Cardiology (ACC), American Heart Association (AHA), the Asia Pacific Heart Rhythm Society (APHRS), and the Society of Thoracic Surgeons (STS): endorsed by the governing bodies of the American College of Cardiology Foundation, the American Heart Association, the European Cardiac Arrhythmia Society, the European Heart Rhythm Association, the Society of Thoracic Surgeons, the Asia Pacific Heart Rhythm Society, and the Heart Rhythm Society. Heart Rhythm 2012; 9: 632-96.e21.*
5. Park JH, Pak HN, Kim SK, Jang JK, Choi JI, Lim HE, Hwang C, Kim YH. *Electrophysiologic characteristics of complex fractionated atrial electrograms in patients with atrial fibrillation. J Cardiovasc Electrophysiol 2009; 20: 266-72.*
6. Shim EB, Leem CH, Abe Y, Noma A. *A new multi-scale simulation model of the circulation: from cells to system. Philos Trans A Math Phys Eng Sci 2006; 364: 1483-500.*
7. Shim EB, Amano A, Takahata T, Shimayoshi T, Noma A. *The cross-bridge dynamics during ventricular contraction predicted by coupling the cardiac cell model with a circulation model. J Physiol Sci 2007; 57: 275-85.*
8. Im UB, Kwon SS, Kim K, Lee YH, Park YK, Youn CH, Shim EB. *Theoretical analysis of the magnetocardiographic pattern for reentry wave propagation in a three-dimensional human heart model. Prog Biophys Mol Biol 2008; 96: 339-56.*
9. Ashihara T, Namba T, Ito M, Ikeda T, Nakazawa K, Trayanova N. *Spiral wave control by a localized stimulus: a bidomain model study. J Cardiovasc Electrophysiol 2004; 15: 226-33.*
10. Ten Tusscher KH, Panfilov AV. *Alternans and spiral breakup in a human ventricular tissue model. Am J Physiol Heart Circ Physiol 2006; 291: H1088-100.*
11. Priebe L, Beuckelmann DJ. *Simulation study of cellular electric properties in heart failure. Circ Res 1998; 82: 1206-23.*
12. Iyer V, Mazhari R, Winslow RL. *A computational model of the human left-ventricular epicardial myocyte. Biophys J 2004; 87: 1507-25.*
13. Ten Tusscher KH, Bernus O, Hren R, Panfilov AV. *Comparison of electrophysiological models for human ventricular cells and tissues. Prog Biophys Mol Biol 2006; 90: 326-45.*
14. Ern A, Guermond J. *Theory and practice of finite elements. New York: Springer, 2004.*
15. Clayton RH, Holden AV. *A method to quantify the dynamics and complexity of re-entry in computational models of ventricular fibrillation. Phys Med Biol 2002; 47: 225-38.*
16. Park JH, Park SW, Kim JY, Kim SK, Jeoung B, Lee MH, Hwang C, Kim YH, Kim SS, Pak HN. *Characteristics of complex fractionated atrial elec-*

trogram in the electroanatomically remodeled left atrium of patients with atrial fibrillation. Circ J 2010; 74: 1557-63.

17. Moe G. On the multiple wavelet hypothesis of atrial fibrillation. Arch Int Pharmacodyn Ther 1962; 140: 183-8.

18. Iyer AN, Gray RA. An experimentalist's approach to accurate localization of phase singularities during reentry. Ann Biomed Eng 2001; 29: 47-59.

19. Oppenheim AV, Schafer RW. Discrete-time signal processing. Upper Saddle River: Prentice-Hall, 1989.

20. Konings KT, Smeets JL, Penn OC, Wellens HJ, Allessie MA. Configuration of unipolar atrial electrograms during electrically induced atrial fibrillation in humans. Circulation 1997; 95: 1231-41.

21. Kienzle MG, Miller J, Falcone RA, Harken A, Josephson ME. Intraoperative endocardial mapping during sinus rhythm: relationship to site of origin of ventricular tachycardia. Circulation 1984; 70: 957-65.

22. Haqqani HM, Kalman JM, Roberts-Thomson KC, Balasubramaniam RN, Rosso R, Snowdon RL, Sparks PB, Vohra JK, Morton JB. Fundamental differences in electrophysiologic and electroanatomic substrate between ischemic cardiomyopathy patients with and without clinical ventricular tachycardia. J Am Coll Cardiol 2009; 54: 166-73.

23. Jalife J, Berenfeld O, Mansour M. Mother rotors and fibrillatory conduction: a mechanism of atrial fibrillation. Cardiovasc Res 2002; 54: 204-16.

24. Wu TJ, Lin SF, Weiss JN, Ting CT, Chen PS. Two types of ventricular fibrillation in isolated rabbit hearts: importance of excitability and action potential duration restitution. Circulation 2002; 106: 1859-66.

25. Pak HN, Oh YS, Liu YB, Wu TJ, Karagueuzian HS, Lin SF, Chen PS. Catheter ablation of ventricular fibrillation in rabbit ventricles treated with beta-blockers. Circulation 2003; 108: 3149-56.

26. Lee G, Roberts-Thomson K, Madry A, Spence S, Teh A, Heck PM, Kumar S, Kistler PM, Morton JB, Sanders P, et al. Relationship among complex signals, short cycle length activity, and dominant frequency in patients with long-lasting persistent AF: a high-density epicardial mapping study in humans. Heart Rhythm 2011; 8: 1714-9.

27. Hodgkin AL, Huxley AF. A quantitative description of membrane current and its application to conduction and excitation in nerve. J Physiol 1952; 117: 500-44.

28. Pak HN, Kim YH, Lim HE, Chou CC, Miyauchi Y, Fang YH, Sun K, Hwang C, Chen PS. Role of the posterior papillary muscle and purkinje potentials in the mechanism of ventricular fibrillation in open chest dogs and Swine: effects of catheter ablation. J Cardiovasc Electrophysiol 2006; 17: 777-83.